IMPROVEMENT OF CROSSFLOW AERODYNAMIC PREDICTIONS FOR FORWARD FLIGHT AT ALL ADVANCE RATIOS

Joachim Hodara Marilyn J. Smith
School of Aerospace Engineering
Georgia Institute of Technology
Atlanta, Georgia, 30332-0150, USA

ABSTRACT

The aerodynamics of rotorcraft in forward flight, particularly at high advance ratios, are highly complex. Of particular interest is the impact of crossflow on forward flight performance that occurs over large portions of the rotor disk. Results from high fidelity numerical experiments on an infinite yawed wing, previously validated with experimental data for a wide range of Mach numbers, angles of attack and yaw angles, are analyzed for use in airfoil tables (C81 tables) for rotorcraft comprehensive codes. Investigation of the errors introduced by interpolation of airfoil tables and application of the Betz crossflow and independence principles in various flight regimes has been completed, including further understanding of the physics driving the behavior of the integrated airfoil performance. The analysis has also been extended to reverse flow conditions, which become significant at high advance ratios. Empirical corrections have been developed that improve the lift, drag and pitching moment predictions of the crossflow model.

NOTATION

a	Lift curve slope (rad^{-1})
AR	Aspect Ratio of the wing
c	Airfoil chord length (m)
D', L'	Sectional drag, lift per unit span (N/m)
C_d	Sectional drag coeff., $C_d = D' / \left(\frac{1}{2}\rho_\infty V_\infty^2 c\right)$
C_l	Sectional lift coeff., $C_l = L' / \left(\frac{1}{2}\rho_\infty V_\infty^2 c\right)$
C_m	Sectional pitching moment coefficient about the quarter chord, $C_m = M' / \left(\frac{1}{2}\rho_\infty V_\infty^2 c^2\right)$
M'	Sectional pitching moment per unit span about the quarter chord (N)
M	Mach number, $M = V/a_\infty$
r	Dimensionless radial distance
R_e	Reynolds number, $R_e = \rho V c/\mu$
u, v, w	x, y and z components of velocity (m/s)
V	Velocity magnitude (m/s)
α	Angle of attack (rad)
Λ	Yaw angle (rad)
μ	Molecular viscosity (Pa.s)
ρ	Density (kg/m^3)
∞	Freestream quantity

1 INTRODUCTION

The maximum speed of conventional rotorcraft has historically been limited to advance ratios below 0.5, based on the impact of retreating blade on the lift and propulsive force. Over the past two decades, significant progress in both hardware and software has sparked new engineering research and development that have the potential to advance the capabilities of conventional concepts. New designs such as the Cartercopter [1] obtain improved efficiency over a wide range of flight speeds, including advance ratios greater than 1.0. This ability to achieve improved efficiency with traditional rotor systems is attractive, but as Harris noted in 2008 [2], most comprehensive rotorcraft codes have typically neglected some of the ramifications of the flow over the rotor disk in these flight conditions, including but not limited to larger regions of transonic, reverse, cross, and stalled flows. Thus, these codes introduce larger errors in the design and analysis of these high speed conditions.

Conventional helicopters flying at high advance ratio experience significant changes in the primary directional component of the flow on the rotor blade for certain azimuthal regions. At $\mu = 0.5$, the entire retreating side of the rotor disk encounters local incoming flow at angles of 30° or larger. As illustrated in Fig. 1, this flow direction increases to 50° when $\mu = 1.0$, resulting in large regions of cross flow where the radial or spanwise component of the flow is comparable to or exceeds the streamwise flow component. In addition, a considerable amount of reverse flow exists on the retreating side of the rotor disk. In this circumstance, the rotor blades operate with the trailing edge in the relative wind so that the blade appears more as a flat plate rather than an airfoil. These effects require investigation and inclu-

Presented at the 40th European Rotorcraft Forum, Southampton, UK, September 2–5, 2014.

sion of improved aerodynamics model to accurately capture these physics as they influence the performance predictions. Following World War II, the im-

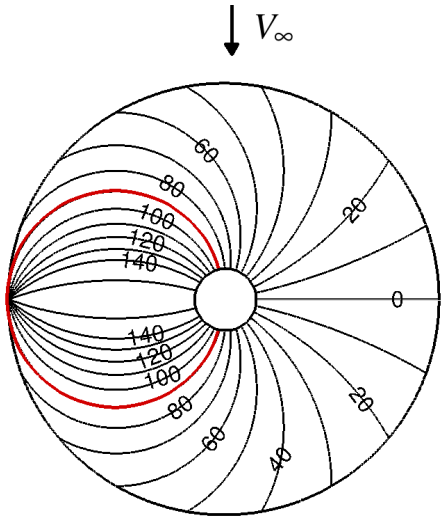

Fig. 1: Iso-sweep angles [deg] over the rotor disk at $\mu = 1.0$ (counter-clockwise rotation). The red line indicates the reverse flow region. From Ref. 3.

pact of cross flow on non-rotating systems was investigated via several experimental studies. Purser and Spearman [4] established an extensive database with yawed finite wings of aspect ratios 3 and 6, including a NACA0012 profile. Their results indicated that the use of the independence principle [5] was justified in calculating the chordwise pressure distribution of yawed wing in the linear regime. Purser and Spearman also observed an unexpected stall delaying phenomenon due to crossflow. Despite this increase in lift, there was no indication of a reduction in the separation drag. These findings were confirmed in the 1980s and 1990s by St. Hilaire [6,7] and Lorber [8] with a NACA0012 and a Sikorsky SSC-A09 profile respectively. Both authors noted substantial deviations from the independence principle for combinations of flight conditions resulting in non-linear interactions such as stall and transonic effects. McCroskey [9] solved the laminar boundary layer equations with small crossflow on a rotating wing. His results confirmed that crossflow effects generally tend to delay separation on the retreating side of the rotor.

Johnson et al. [10] and Harris [2] recently explored the ability of five comprehensive rotorcraft codes to predict rotor power at high advance ratio. Harris concluded after detailed examination of the data indicated that *"not one of the codes can predict to engineering accuracy above an advance ratio of 0.62 the control positions and shaft angle of attack required for a given lift."* Harris investigated high advance ratios, but could not validate his predictions due to the lack of experimental data for advance ratios above 1.0.

In addition to exploring the aerodynamics of high-advance-ratio flight, the present study aims at probing the potential of computational experiments as meaningful rotor data. In 2008, Harris [2] suggested that researchers measure the performance of a full-scale rotor in a wind tunnel to at least an advance ratio of 2.5. Since 2008, there have been two sets of high-aspect-ratio wind tunnel tests on a three-bladed NACA0012 rotor [11,12] and the UH-60 four-bladed rotor [13], which have been accompanied by some computational analyses, for example (but not limited to) Refs. 14, 15. These comprehensive analyses indeed indicate that there are discrepancies in the performance predictions as the advance ratio increases.

Based on these recent experimental and numerical experiments, a numerical dataset [3,16] that was previously used to examine the NACA0012 and SC1095 airfoils in reverse and crossflow has been revisited. Present studies were structured to analyze the fundamental physics and corrections needed for airfoil tables (C81 tables) when large regions of reverse and crossflow are present, such as in high-advance-ratio flight. In this work, airfoil table interpolation errors, as well as the accuracy of reverse and crossflow performance methods at low angles of attack across the range of subsonic and transonic flows has been examined. Behavior of these prediction models at large angles of attack (stall and post stall) is underway and will be presented in another paper. Both the NACA0012 and SC1095 airfoils have been examined, but the NACA0012 results are presented for brevity. However, all differences in the physical or modeled behavior of the SC1095 airfoil are noted.

2 COMPUTATIONAL MODEL

A large numerical database was generated for an infinite NACA0012 wing in crossflow [3,16]. The NACA0012 airfoil is a seminal test configuration, for which an extensive experimental database exists [17]. The numerical simulations were conducted for a single Reynolds number at both incompressible and compressible speeds up to a Mach number of 1.0. The present study concentrates on the behavior a low angles of attack between 0°–8°, with yaw angles ranging from 0° to 80°. The exact simulation conditions are summarized in Table 1. The angles of attack of 172° and 176° are comparable low angles of attack under reverse flow conditions.

2.1 Numerical Methods

The numerical simulations were conducted using OVERFLOW (2.0y and 2.1z), a structured solver with Chimera overset grid capabilities [18]. The spatial terms were discretized using a fourth-order central difference algorithm incorporating a diagonalized Beam-Warming scalar pentadiagonal scheme. Second-order temporal integration was achieved by

applying Newton subiterations to a first-order implicit Euler scheme. Artificial dissipation was included using the spectral-based dissipation scheme. The fourth- and second-order smoothing parameters were respectively 0.04 and 0.0 for subsonic flow, while the second-order smoothing was increased to 0.2 for transonic flows with shocks.

Table 1: Summary of the simulation database.

Mach Number	M	0.2, 0.3, 0.6, 0.7, 0.8
Reynolds Number	R_e	5.10^6
Sweep Angle	Λ	0° to 80° (10° steps)
Angle of Attack	α	0°, 4°, 8°, 172°, 176°

A hybrid unsteady Reynolds-averaged Navier-Stokes (URANS) and large eddy simulation (LES) turbulence model [19] was applied to ensure accurate unsteady predictions. The URANS approach is based on the two-equation $k-\omega$ shear stress transport (SST) model of Menter, which incorporates statistical methods to model the entire turbulent length and time scale spectrum. RANS/URANS turbulence models have been widely utilized for aerospace applications due to their low computational cost and reasonable predictions of attached flows. For some three-dimensional applications such as a wing in cross flow, URANS turbulence models have been shown [3] to fail at capturing flow features essential to accurately predict the flow physics and aerodynamic characteristics. An alternative for computing the flow solution is called large eddy simulation (LES). The large scales of turbulence are resolved, while the smaller scales are modeled. The sub-grid scale (SGS) model employed in the present study is the model of Kim & Menon, which governs the transport of SGS turbulent kinetic energy. Because of its high computational cost, LES should only be used when URANS models are inadequate. The simple regions of the flow (attached boundary layers, etc) are therefore modeled using URANS methods, while the more complex flow features (separation, etc) are captured using LES. The two approaches are combined using a blending function that ensures a smooth transition from one model to the other. This URANS/LES hybridization has recently been validated over a wide range of applications involving massive separation and unsteady effects [20,21].

2.2 Computational Grids

A structured grid modeled the wings under consideration. This mesh was generated by Smith et al. [3,22] for analyzing the behavior of wings at high and reverse angles of attack. This previous article includes grid refinement studies for angles of attack ranging from 0° to 180°. The mesh was generated with an O-grid topology, for the purpose of capturing the finite trailing edge. It is important to maintain a high fidelity at the trailing edge in order to study the effect of yaw in reverse flow, as demonstrated in Smith et al. [3,22].

The NACA0012 grid consists of 120 points normal to the airfoil and 825 circumferential points, with 20 of those being located along the blunt trailing edge. The streamwise points were distributed equally over the upper and lower surfaces of the airfoil. The initial cell spacing at the wall was chosen to ensure that $y^+ < 1$ at the Reynolds number considered in this study (see Table 1) and that 35-50 normal cells resolve the boundary layer [22,23]. The grid extent from the airfoil to the outer boundary was progressively increased until convergence of the integrated forces and moments was obtained. This corresponded to an outer boundary distance of $18c$. The SC1095 grid was developed using the NACA0012 grid as a guide.

To model crossflows, it is critical to determine the span dimension required to accurately capture the three-dimensional nature of the semi-infinite flow without interference from the period spanwise boundary conditions. Three different grids with spans $2c$, $4c$ and $8c$ were evaluated. An analysis of the vorticity fields revealed that a spanwise extent of $2c$ with 61 span stations was sufficient for angles of attack below stall for both forward and reverse flows.

3 EXPERIMENTAL VALIDATION

There are few data sets available to correlate high Mach numbers yawed wing results. Much of the experimental data are specific to certain planforms and are thus difficult to generalize for the present study. Purser and Spearman [4] conducted an extensive experimental investigation on finite wings in crossflow, including a NACA0012 profile of aspect ratio six. However, this study was limited to incompressible Mach numbers. The present numerical results [3,16,22] were therefore validated in two steps. First, the incompressible NACA0012 yawed results were correlated to the extensive experimental database of Purser and Spearman [4]. Then, the compressible NACA0012 and SC1095 at zero yaw angle ($\Lambda = 0^\circ$) results were correlated to the experimental data of McCroskey [17] and Bousman [24]. In addition to the prior grid independence assessment, best practices in the literature indicate that CFD predictions are reliable if the computational results correlate well with these two data sets.

3.1 Incompressible Yawed Wing

The incompressible NACA0012 yawed results were compared to the extensive database of Purser and Spearman [4]. The experiments were conducted over a range of Reynolds number from $R_e = 0.992 \times 10^6$ to 1.25×10^6 with an aspect ratio of six. The impact of Reynolds number on the lift curve slope was observed

to be negligible at low angles of attack before the onset of stall [4]. The following correction was applied to account for the influence of the wing finite tip.

$$(1)\quad a = \frac{a_0 \cos\Lambda}{\sqrt{1 + \left[\left(a_0 \cos\Lambda\right)/\left(\pi AR\right)\right]^2} + \left(a_0 \cos\Lambda/\left(\pi AR\right)\right)}$$

where a is the corrected lift curve slope and a_0 is the uncorrected slope. AR and Λ are respectively the aspect ratio and the sweep angle of the wing. This correction was developed by Kuchemann [25] specifically for swept wings. Figure 2 shows the computationally-predicted normalized lift curve slope $a/a_{(\Lambda=0)}$ of the NACA0012 yawed section at $M = 0.2$ correlated with the experimental data. The CFD solver predicts the experimental lift curve slope within 2% for yaw angles up to 50°. Beyond this angle, the error slightly increases and reaches 9% when $\Lambda = 80^\circ$. The results are also in very good agreement with the independence principle, which predicts that $a = a_{(\Lambda=0)} \cos^2\Lambda$.

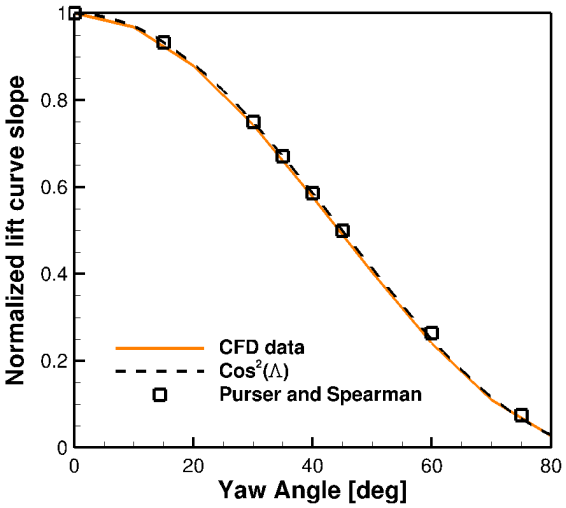

Fig. 2: Correlation of the normalized lift curve slope (NACA0012 yawed section) of computational (CFD) results at $M = 0.2$ [3] with the M=0.1 experimental data of Purser and Spearman [4]

Unfortunately, the quality of the drag polar published by Purser and Spearman was poor, preventing direct drag comparisons. According to the independence principle, the drag is only slightly affected by the crossflow [5]. Hence, only the at zero yaw validation for the drag coefficients will be sufficient for the present study.

3.2 Compressible Wing at Zero Yaw Angle

The lift curve slope and drag coefficient (at $\alpha = 0^\circ$) for the NACA0012 at zero yaw wing were correlated to the experimental data gathered by McCroskey [17]. McCroskey examined a large body of experimental results, collected in more than 40 wind tunnels on NACA0012 wings. The comparison with the present computational simulations are shown in Fig. 3. The experimental data shown in this plot were obtained at Reynolds numbers on the order of 10^6. The computational predictions fall within the experimental error bounds for both the lift curve slope and drag coefficient. Similar results were observed for the pitching moment and the aerodynamic coefficients for the SC1095 airfoil [22].

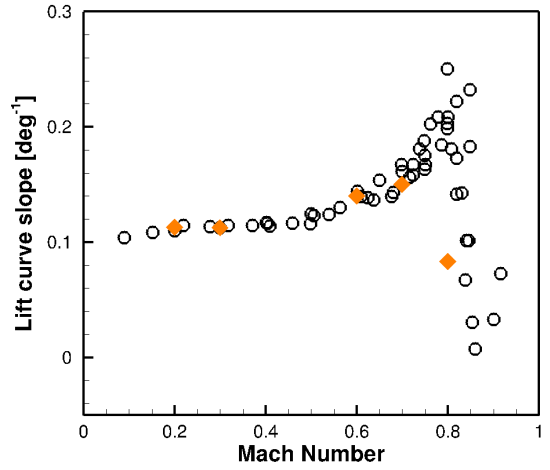

(a) Lift curve slope vs. Mach number

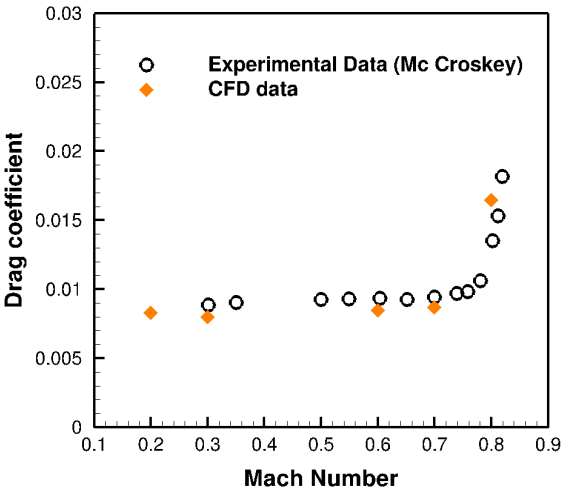

(b) Drag coefficient at $\alpha = 0^\circ$ vs. Mach number

Fig. 3: Correlation of the computational results (zero yaw NACA0012 airfoil) with the experimental data of McCroskey [17].

4 CROSSFLOW AND YAW INDEPENDENCE MODELS

The vast majority of comprehensive rotorcraft codes rely on the independence principle to account for crossflow effects. This approach assumes that the aerodynamics of the blade is solely affected by the velocity component in the plane normal to the span,

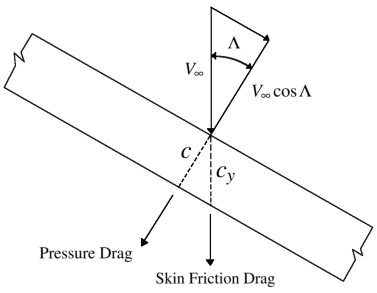

Fig. 4: Independence principle applied to an infinite yawed wing.

and that the properties at each radial station are not affected by the crossflow [26]. The independence principle can be derived from the boundary layer equations. Considering a cylindrical wing of infinite aspect ratio swept at an angle Λ, all derivatives along the radial direction must vanish. Although there may exist a radial flow v, all properties cannot be functions of the radial direction y. It directly follows that pressure gradients can only act in the direction normal to the span axis, as illustrated in Fig. 4. The compressible steady boundary layer equations for laminar flow in Cartesian coordinates can be written as

$$\frac{\partial}{\partial x}(\rho u)+\frac{\partial}{\partial z}(\rho w)=0 \tag{2}$$

$$\rho\left(u\frac{\partial u}{\partial x}+w\frac{\partial u}{\partial z}\right)=-\frac{dp}{dx}+\frac{\partial}{\partial z}\left(\mu\frac{\partial u}{\partial z}\right) \tag{3}$$

$$\rho\left(u\frac{\partial v}{\partial x}+w\frac{\partial v}{\partial z}\right)=\frac{\partial}{\partial z}\left(\mu\frac{\partial v}{\partial z}\right) \tag{4}$$

$$\rho\left(u\frac{\partial H}{\partial x}+w\frac{\partial H}{\partial z}\right)=\frac{\partial}{\partial z}\left[\mu\frac{\partial}{\partial z}\left(H+\frac{P_r-1}{P_r}C_pT\right)\right] \tag{5}$$

where P_r is the Prandtl number and H is the stagnation enthalpy. The z-momentum equation reduces to $\partial p/\partial z \simeq 0$ because of the boundary layer approximation. If the flow is incompressible, the above system of equations is decoupled. Eqs. (2) and (3) can be solved for u and w, without regard to the crossflow v. The independence principle does not hold for compressible flow, where density becomes a function of both u and v [27]. There has also been much debate regarding the applicability of the independence principle to turbulent flow. Recent results by Wygnanski [28] suggest that the independence principle applies to laminar and (Reynolds-averaged) turbulent boundary layers alike.

Mathematically, the independence principle can be used to relate the lift and drag coefficients of the yawed wing to the two-dimensional at zero yaw airfoil characteristics. The forces acting on the wing can be seen either in terms of sections aligned with the freestream (yawed section, denoted by the subscript y), or sections normal to the leading edge (normal sections, no subscript). As illustrated in Fig. 4, the characteristics of the yawed and normal sections can be related using simple geometry:

$$q=q_y\cos^2\Lambda \qquad c=c_y\cos\Lambda \qquad \alpha=\frac{\alpha_y}{\cos\Lambda}, \tag{6}$$

where q is the dynamic pressure, c is the chord and α is the angle of attack. It is generally assumed that the drag on the wing is aligned with the freestream [29]. The lift and drag coefficient for the yawed and normal sections can therefore be related as follows:

$$c_l(\alpha)=\frac{L}{qS}=\frac{L_y}{(q_y\cos^2\Lambda)S}=\frac{c_{l_y}(\alpha_y)}{\cos^2\Lambda} \tag{7}$$

$$c_d(\alpha)=\frac{D}{qS}=\frac{D_y\cos\Lambda}{(q_y\cos^2\Lambda)S}=\frac{c_{d_y}(\alpha_y)}{\cos\Lambda}. \tag{8}$$

The reference area does not change for the yawed and normal sections, since an increase in span is compensated by a corresponding reduction in chord length. Up to this point, the independence principle has not been applied as Eqs. (7) and (8) arise from geometric considerations, as well as a few assumptions (drag aligned with the freestream, etc). According to the independence principle [5], the pressure distribution in the direction normal to the span is not influenced by the crossflow:

$$c_l(\alpha)=c_{l_{2D}}(\alpha). \tag{9}$$

Also, the boundary layer grows in the freestream direction without being influenced by the crossflow:

$$c_{d_y}(\alpha_y)=c_{d_{2D}}(\alpha_y). \tag{10}$$

Equations (9) and (10) define the independence principle. When Eqs. (9) and Eq. (10) are introduced into Eq. (7) and Eq. (8), the normal aerodynamic coefficients can be directly related to the two-dimensional at zero yaw airfoil characteristics, and the crossflow model is obtained:

$$c_l(\alpha)=\frac{c_{l_{2D}}\left(\alpha\cos^2\Lambda\right)}{\cos^2\Lambda} \tag{11}$$

$$c_d(\alpha)=\frac{c_{d_{2D}}\left(\alpha\cos\Lambda\right)}{\cos\Lambda}. \tag{12}$$

It is important to notice that Eqs. (11) and (12) differ from the independence principle. Crossflow models are typically written in this form [29] in order to capture the lift loss delay observed experimentally on yawed wings [30]. When interpolating in airfoil tables, the coefficients are evaluated at the normal Mach number $M=M_\infty\cos\Lambda$. The change in thickness between the yawed and normal sections could also be considered ($t_y=t\cos\Lambda$), but is generally neglected in comprehensive rotorcraft codes [29].

4.1 Airfoil Table Interpolation

The crossflow model described in the previous section relies on two-dimensional airfoil characteristics. These parameters are typically stored in airfoil tables, which contain the aerodynamic coefficients for a given set of Mach numbers and angles of attack obtained through experiments, computations, aerodynamic theory, or a combination of these. Comprehensive codes typically utilize linear interpolation schemes to rapidly estimate the coefficients at the local rotor conditions. This approach is fast and robust but lacks accuracy in highly non-linear regions, as illustrated in Fig. 5 for the areas $M \in [0.7, 0.8]$ and $M \in [0.9, 1.0]$. Third-order interpolations can also be used, but sometime lead to oscillations or overshoots in the surrogate model [31], as can be seen in Fig. 5. Radial Basis Functions (RBF) do not have the issues identified in these polynomial basis functions, and are widely used to construct the surrogate models of functions given a set of discrete data points. A multiquadric radial basis function was chosen to interpolate the coefficients, based on prior results with aerodynamic data [32]. Once the RBF model has been trained, it becomes possible to interpolate the function at any point in the domain. As illustrated in Fig. 5, the RBF captures the non-linear region without generating oscillations resulting from higher-order polynomial interpolations. Linear polynomial methods are accurate below $M = 0.7$ in this example, but cannot capture the sharp rise in drag coefficient that occurs at higher Mach numbers. The relative error between the RBF and linear polynomial interpolations is relatively small at most Mach numbers, but it becomes significant (50% error) when the critical Mach number is reached.

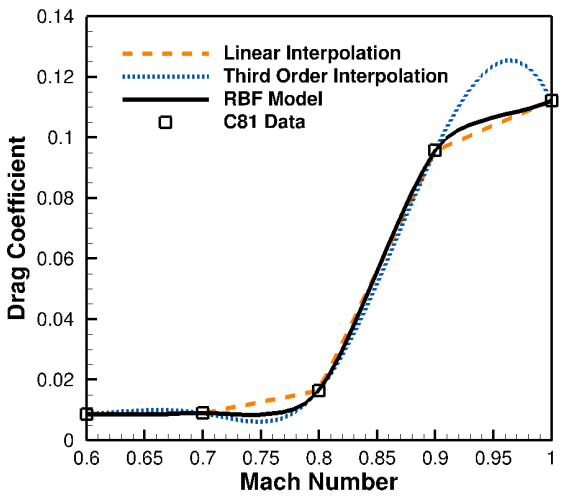

Fig. 5: Interpolation of the drag coefficient of an at zero yaw NACA0012 wing at $\alpha = 0^\circ$ using different schemes.

The implementation of interpolation algorithms in comprehensive rotorcraft codes requires special treatment in order to maintain a low computational cost. During the design phase of a new concept, thousands of configurations are evaluated and compared. It is therefore of the utmost importance to keep the interpolation time as low as possible. Linear and third-order polynomial schemes are typically simple enough so that their weights w_i can be computed analytically. The additional training step does not represent a major issue for RBF methods, since this training only needs to be completed once for any particular airfoil table. Without regard to the training time, the interpolation time is directly related to the number of basis functions (n) retained in the model [31]. The polynomial basis of linear schemes consists of only three elements in two dimensions, so that the computational cost is very low. However, RBF methods require one basis function per sample point in the model. The interpolation cost therefore increases dramatically with the extent of the surrogate model. For the present simulation, it was found that a RBF model trained with 55 points (11 Mach numbers and 5 angles of attack) required twice as much time as a linear polynomial scheme to interpolate a data point. This factor increased to 10 for a model sampled with 220 points. However, the RBF methods can be used in a different way. Because experimental or computational methods tend to be relatively sparse, the RBF method can be utilized to generate airfoil tables with a finer resolution so that interpolations using linear polynomial schemes are nominally error free in regions of rapid change.

5 RESULTS AND DISCUSSION

A sweep of Mach numbers ($M = 0.2$ - 0.8) and angles of attack ($\alpha = 0^\circ$ - 8°) for yawed flow from $\Lambda = 0^\circ$ - 80° for the NACA0012 and SC1095 was compared with the crossflow model in Eq. (11) and Eq. (12). The lift, drag and pitching moment coefficients are successively analyzed in this angle of attack region for infinite uniform wings comprised of the two airfoils. The analysis has then been extended to reverse flow conditions, where the blade operates with the trailing edge forward in the relative wind. As noted previously, the results are shown for the NACA0012 airfoil, with commentary included for differences in the SC1095 airfoil results where applicable.

5.1 Lift Coefficient

Figure 6 illustrates a typical comparison between the computational results and the crossflow model. As the independence principle states that the pressure distribution normal to the span axis is not influenced by the cross flow, the sectional lift coefficient for a normal section should therefore be constant for the range of yaw angles considered. This assumption is

largely verified by the present numerical experiments at $\alpha = 4°$, as illustrated in Fig. 6(a). The simple crossflow model provides excellent results, with relative errors consistently within 5% of the computational data. The lift of the at zero yaw wing increases with Mach number due to compressibility effects, until it reaches the divergence Mach number and drops suddenly. The loss in lift from shock-induced boundary layer separation can also be observed in Fig. 3 by the change in slope at $M = 0.8$. As the sweep angle increases, the normal Mach number decreases and the wing progressively leaves the transonic regime. Figure 6(b) illustrates the same comparison at an higher angle of attack $\alpha = 8°$. The independence principle provides results within 9% of the computational data in the incompressible regime. However, the crossflow model constantly overpredicts the lift coefficients up to 45% at higher Mach numbers.

The source of these discrepancies has been investigated. At this point, it is important to distinguish the differences between the crossflow model and the actual independence principle. The latter states that the lift coefficient of the normal section is unaffected by yaw angle. On the other hand, the crossflow model described in Eq. (11) was developed to account for the delay in boundary layer separation. The reduction of the effective angle of attack by $\cos^2\Lambda$ in Eq. (11) artificially increases the maximum stalling angle and lift coefficient, as observed in early experiments [33]. These features are desirable at low Mach numbers, but appeared to generate signifant errors in the transonic regime, where the flow is highly non-linear. In order to verify this hypothesis, the lift coefficients predicted by both the independence principle (Eq. (9)) and the crossflow model (Eq. (11)) were correlated against the numerical experiments. Figure 7 demonstrates that the independence principle still holds in the transonic regime. The coefficient at $M = 0.8$ is predicted within 7% of the CFD data over the entire range of yaw angles, where errors greater than 45% were observed with the crossflow model. Both the independence principle and crossflow model have strengths and weaknesses. The independence principle holds in the transonic regime, but it will not predict the delay in lift loss observed experimentally at subcritical Mach numbers [30]. The crossflow model should only be used when the Mach number normal to the span axis is below the critical Mach number.

As noted previously, Jones [26] and other authors derived the three-dimensional laminar boundary layer equations with crossflow. They concluded that the independence principle would fail at compressible speed, because of the effect of the radial velocity v on density. However, the present results clearly show that the independence principle holds in the compressible regime. This conclusion is not surprising, as there are several concepts that justify this observation. The approach consisting of deriving the full boundary layer equations is the most rigorous one.

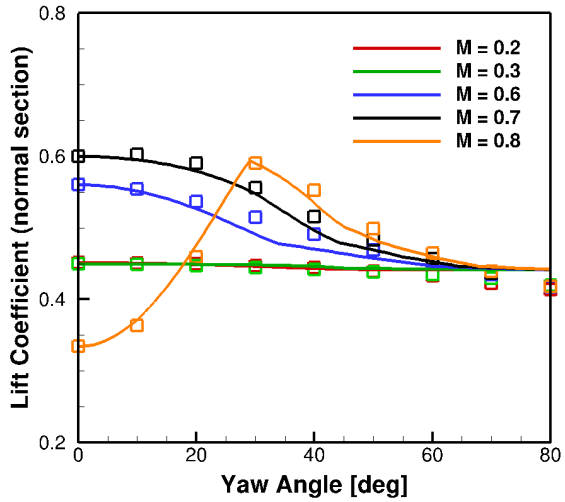

(a) $\alpha = 4°$

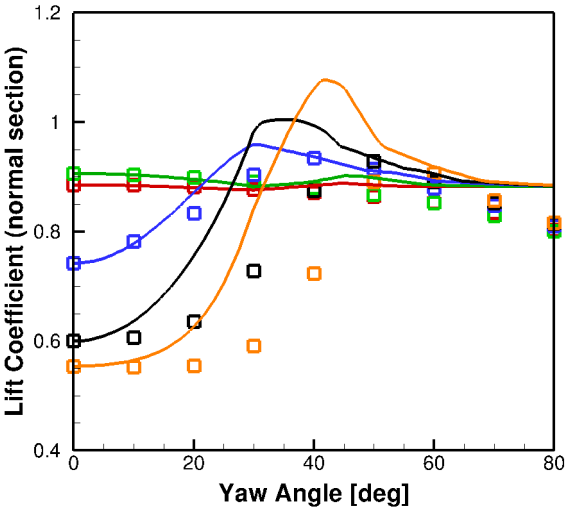

(b) $\alpha = 8°$

Fig. 6: Correlation of the CFD lift coefficient (symbols) with the crossflow model (solid lines) at different Mach numbers and yaw angles.

However, a second justification is often presented in the rotorcraft literature [29]. Consider an infinite uniform wing at zero yaw (see Fig. 4) with an incoming freestream $V_\infty \cos\Lambda$ normal to the leading edge. If the uniform wing was moving at a velocity $V_\infty \sin\Lambda$ parallel to the leading edge, the normal pressure distribution at any span station would remain unaffected. This is again the independence principle.

5.2 Drag Coefficient

The drag coefficients predicted by the crossflow model are correlated with the numerical experiments at several Mach numbers and yaw angles. The behavior is similar at both angles of attack shown in Fig.

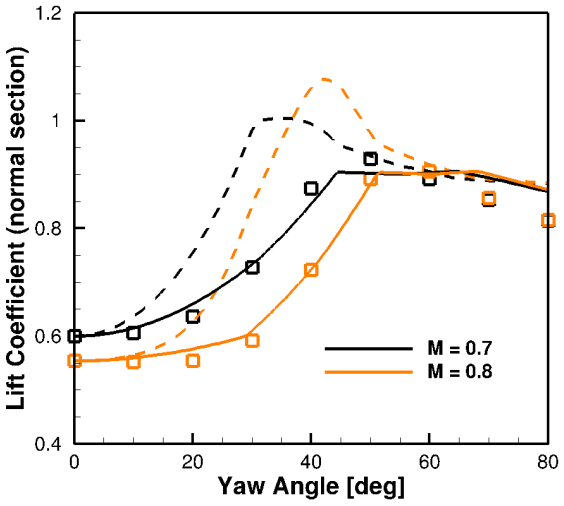

Fig. 7: Correlation between the crossflow model (dash lines), the independence principle (solid lines) and the numerical experiments (symbols).

8. The crossflow model performs very well below a yaw angle of approximately $\Lambda = 40°$, with predictions typically within 10% of the computational data. Above this angle, the drag coefficient becomes almost independent of Mach number. As the yaw angle increases, the normal Mach number reduces, the wing eventually leaves the transonic regime and the wave drag disappears.

At angles of attack where the flow remains attached and in the subcritical Mach range, drag is primarily due to skin friction at the wall. The drag is essentially independent of the angle of attack, which explains the reason why the curves coalesce in Fig. 8. The crossflow model predicts that the skin friction drag of the yawed section will remain constant and independent of the sweep angle. As a result, the drag coefficient for the normal section should increase as $\cos^{-1}\Lambda$, since $c_{d_y}(\alpha_y) = c_d(\alpha)\cos\Lambda$ and the drag coefficient is not influenced by the angle of attack. This leads to large normal drag coefficients when Λ approaches $90°$. This singular point does not arise from unphysical behavior, but from the actual definition of the drag coefficient for the normal section. As the yaw angle approaches $\Lambda = 90°$, the normal component of the velocity vector progressively goes to zero. However, the skin friction drag on the wing remains finite. The drag coefficient for the normal section is now singular due to the definition of an inappropriate reference scale.

This behavior was also noted previously by Smith et al. [3]. The drag coefficient was plotted for the normal sections rather than the yawed sections. The reason behind this choice is that comprehensive rotorcraft codes are based on the drag coefficients for the normal sections when computing the rotor performance. In order to investigate the error introduced by the crossflow model, it is therefore required to remain within this frame of reference.

There has been much debate regarding the applicability of the independence principle for predicting skin friction drag in turbulent boundary layers. Altman and Hayter [34] measured and compared the boundary layer growth for wings with $(45°)$ and without $(0°)$ yaw. They observed a more rapid growth rate for the swept wing, but attributed this result to the differences in the surface conditions of their two models. Hence, Altman and Hayter concluded that the independence principle was valid at moderate lift coefficients. Ashkenas and Riddell [35] also investigated this phenomenon both theoretically and experimentally: "*The conclusion at this point is unmistakable: The independence principle cannot be applied to the case of turbulent boundary layers on yawed flat plates. The measured growth curve, for the case* $\Lambda = 30°$ *and* $45°$ *is thicker than that for the at zero yaw-plate case.*"

The present results bring a new perspective to this debate. As illustrated in Fig. 8, the independence principle remains within 10% of the numerical experiments up to approximately $\Lambda = 40°$. Beyond that point, the crossflow model fails to predict the drag coefficient accurately. At $\Lambda = 80°$ and $\alpha = 4°$, the model over predicts the skin friction by approximately 60%. This error is largely amplified by the projection of the drag coefficient on the normal section, as explained previously and as illustrated in Fig. 4. These results suggest that the crossflow does indeed affect the boundary layer and reduce the skin friction at the wall, as suggested by Ashkenas and Riddell [35]. However, a detailed analysis of the data offered another alternative: the independence principle still holds, but Reynolds number effects need to be considered.

It was assumed that the boundary layer was growing only in the freestream direction, independent of crossflow effects. However, the chords of the yawed and normal sections are different $(c = c_y \cos\Lambda)$, leading to different Reynolds numbers per section. A simple correction based on Prandtl's theory for turbulent boundary layers can be developed to account for this assumption. Assuming a $1/7$ power law for the velocity profile, the classical result for the drag coefficient on a flat plate of length x is:

$$C_d = \frac{0.074}{R_e^{1/5}} \qquad \text{with} \qquad R_e = \frac{U_\infty c}{\nu}, \tag{13}$$

where U_∞ is the freestream velocity and ν is the kinematic viscosity of the flow. In this case, the Reynolds number is based on the normal section chord length. In the swept wing case, the boundary layer will grow in the direction of the freestream, so that the Reynolds number becomes

$$R_{e_y} = \frac{U_\infty c_y}{\nu} = \frac{1}{\cos\Lambda}\frac{U_\infty c}{\nu} = \frac{R_e}{\cos\Lambda}. \tag{14}$$

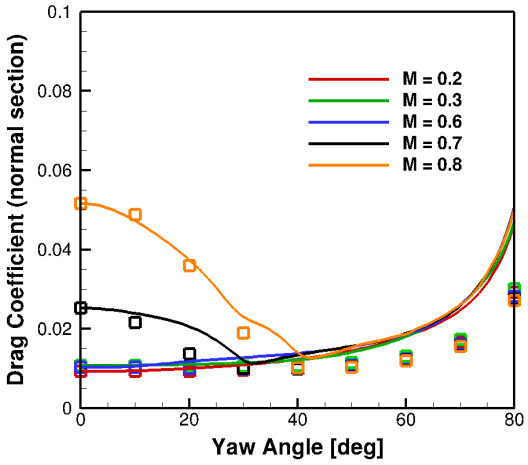

(a) $\alpha = 4^\circ$

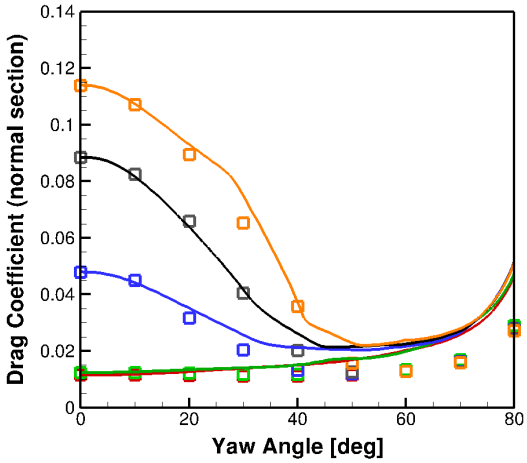

(b) $\alpha = 8^\circ$

Fig. 8: Correlation of the CFD drag coefficient (symbols) with the crossflow model (solid lines) at different Mach numbers and yaw angles.

Introducing the yawed Reynolds number in the formula for the skin friction drag, the following relation can be obtained:

$$C_{d_y} = \frac{0.074}{R_{e_y}^{1/5}} = \frac{0.074}{(R_e/\cos\Lambda)^{1/5}} = C_{d_{2D}} \cos^{1/5}\Lambda. \tag{15}$$

This simple analysis suggests that the drag coefficient of the yawed section will decrease with increasing sweep angle. This conclusion is a direct consequence of the larger Reynolds number due to the projection length. In order to verify this assumption, the crossflow model described in Eq. (12) was modified:

$$c_d(\alpha) = \frac{c_{d_y}(\alpha\cos\Lambda)}{\cos\Lambda} = \frac{c_{d_{2D}}(\alpha\cos\Lambda)}{\cos^{4/5}\Lambda}. \tag{16}$$

This very simple correction significantly improved the drag predictions at high yaw angles, as illustrated in Fig. 9. At $\Lambda = 80^\circ$ and $\alpha = 4^\circ$, the relative error between the crossflow model and the numerical experiment was reduced from 60% to 12%. Further analysis is warranted on different airfoil shapes beyond these two (NACA0012 and SC1095), and what turbulent power law most appropriately holds for rotor operational conditions.

5.3 Pitching Moment Coefficient

The pitching moment coefficient can also be computed from the independence principle. The coefficient at the quarter chord for the normal section can be related to the two-dimensional airfoil characteristics as follows [36]:

$$c_m(\alpha) = c_{m_{2D}}(\alpha\cos^2\Lambda). \tag{17}$$

Figure 10 shows the correlation between the numerical experiments and the crossflow model described in

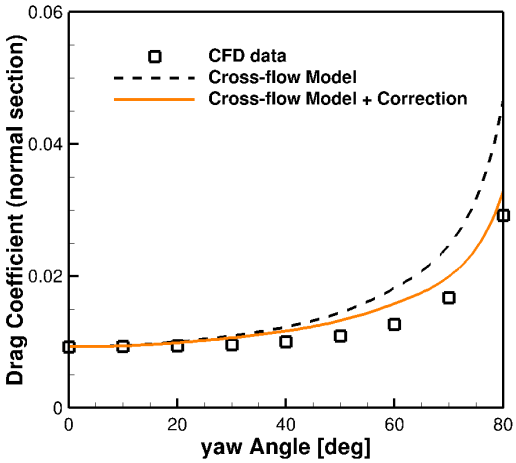

Fig. 9: Normal Drag Coefficient at zero angle of attack and $M = 0.2$ with and without correction term for the boundary layer growth.

Eq. (17). The model exhibits significant discrepancies at high Mach numbers, with relative errors regularly above 50% at $M = 0.8$. The discrepancies are concentrated in the transonic yawed regime. This result is not surprising since the pitching moment is characterized by the pressure distribution about the airfoil. As noted previously, the crossflow model assumptions break down in the transonic regime, introducing large discrepancies in the lift predictions. If the pressure distribution is obtained using the independence principle (Eq. (9)), the errors immediately drop over the whole range of Mach numbers and sweep angles considered, as illustrated in Fig. 10.

The conclusions for the pitching moment are thus similar to the conclusions for the lift coefficient: the independence principle can predict the pitching moment typically within 10% of the numerical experi-

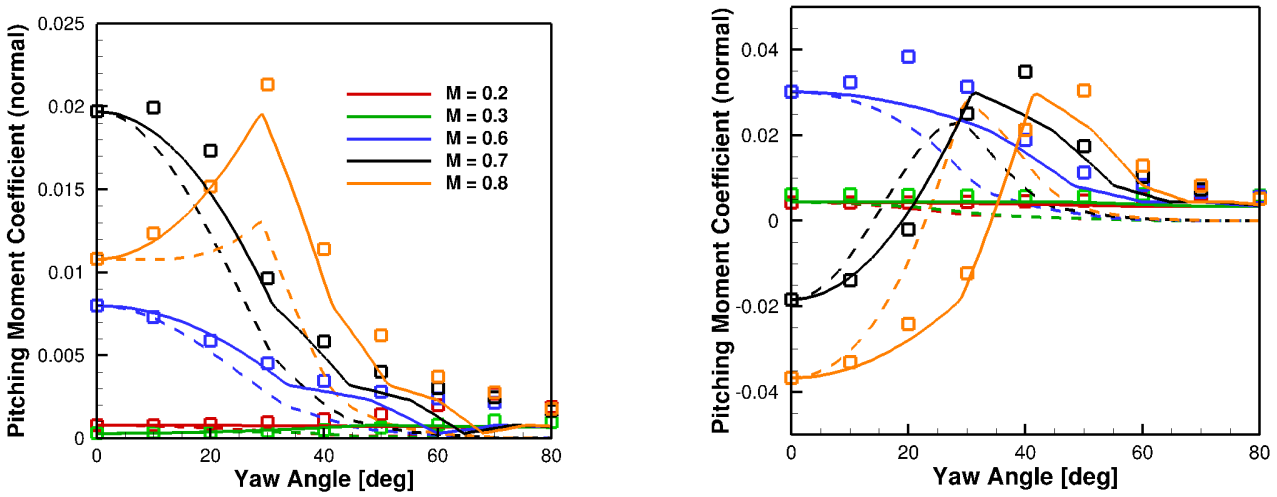

(a) $\alpha = 4^\circ$ (b) $\alpha = 8^\circ$

Fig. 10: Correlation of the CFD pitching moment coefficient about the quarter chord (symbols) with the crossflow model (dash lines) and independence principle (solid lines) at different Mach numbers and yaw angles.

ments, whereas the crossflow model fails in the transonic regime. This failure is due to the large nonlinearities beyond the critical Mach number, and apply to both the symmetric and cambered airfoils evaluated in this study.

5.4 Reverse Flow Aerodynamics

As illustrated in Fig. 1, a considerable amount of reverse flow exists on the retreating side of the rotor disk. In this region, the blades operate with the trailing edge forward in the relative wind. The lift and drag coefficients of infinite wings were investigated at various Mach numbers and yaw angles at $\alpha = 176^\circ$ and 172°. These two angles of attack correspond respectively to 4° and 8° in reverse flow. Both angles of attack exhibited similar features, so that only the results at $\alpha = 172^\circ$ will be presented in Fig. 11.

The incompressible lift coefficient only changes by approximately 10% over the entire range of sweep angles evaluated in this study (0° to 80°). This result is not surprising, since the independence principle should theoretically hold for any cylinder. However, the independence principle assumptions are violated if the boundary layer separates, since the inviscid hypothesis breaks down. The infinite yawed wing in reverse flow was found to behave similarly to a flat plate, as illustrated in Fig. 12. The boundary layer is already separated at the leading edge at only 8° due to the shape of the blunt trailing edge. Significant vorticity is shed from the leading edge separation. As the yaw angle increases, the stall delaying phenomenon observed by Sweet [30] clearly reduces the amount of separation at the trailing edge. Interestingly, this stall delaying effect does not influence the lift coefficient of the wing, as shown in Fig. 11. Hence, it can be reasonably assumed that most of the lift produced by the airfoil in reverse flow comes from the high pressure region on its lower surface. The upper surface is relatively flat, so that there is no significant acceleration of the flow as observed on classical airfoil shapes, both for symmetric and mildly cambered configurations.

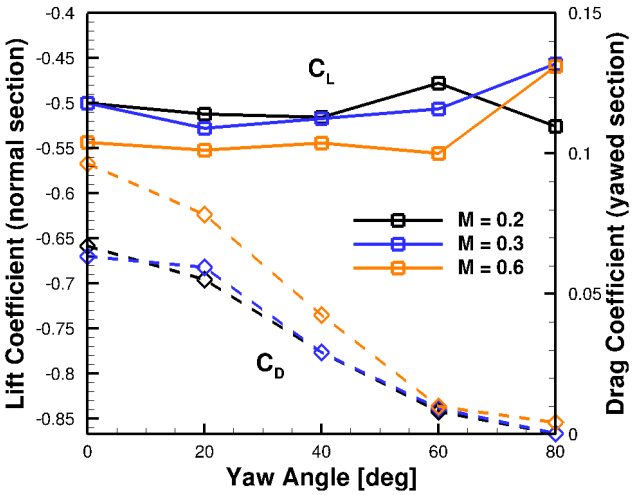

Fig. 11: Lift (solid lines) and drag (dash lines) coefficients of an infinite NACA0012 wing in reverse flow ($\alpha = 172^\circ$) at various Mach numbers and yaw angles from computational simulations.

On the other hand, the drag coefficient is dramatically influenced by the crossflow, reducing from 0.06 at $\Lambda = 0^\circ$ to 0.0003 at $\Lambda = 80^\circ$ (at $M = 0.3$). The independence principle predicts that the boundary layer should grow in the direction of the free stream, without

being influenced by the crossflow. The present results suggest that this assumption does not hold in reverse flow. The reason for this failure can be understood by decomposing the drag into viscous and pressure effects. Pressure drag represents 97% of the total drag force at $\alpha = 172°$, $M = 0.6$ and $\Lambda = 0°$. This contribution reduces to 10% as the yaw angle is increased to $\Lambda = 80°$. As illustrated in Fig. 12, the crossflow significantly reduces the boundary layer separation at the trailing edge of the wing.

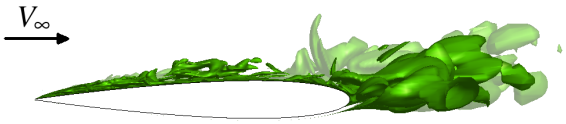

(a) Yaw angle $\Lambda = 0°$

(b) Yaw angle $\Lambda = 80°$

Fig. 12: Spanwise vorticity iso-surface ($\omega_y = 5$). Stall delaying effect of cross flow on a NACA0012 infinite wing in reverse flow ($M = 0.6$, $\alpha = 172°$).

Recalling the theory of infinite uniform wings, there can be no pressure gradient in the radial direction. The pressure drag will necessarily act in the direction normal to the span axis, which is in direct contradiction with the crossflow model assumptions. Following the approach proposed by Harris [5], one can derive an approximation for the pressure drag below stall. The drag force normal to the span axis is given by

$$D_p = \frac{1}{2}\rho \left(V_\infty \cos\Lambda\right)^2 S c_{d_{p_{(\Lambda=0)}}}, \tag{18}$$

where $C_{d_{p_{(\Lambda=0)}}}$ is the pressure drag coefficient for the at zero yaw wing. As shown in Fig. 4, the pressure drag will act in the direction normal to the span axis. It follows that the component of the drag force parallel to the freestream is

$$D_{p_y} = D_p \cos\Lambda = \frac{1}{2}\rho V_\infty^2 \cos^3\Lambda S c_{d_{p_{(\Lambda=0)}}}. \tag{19}$$

Combining Eq. (18) and Eq. (19), the pressure drag coefficient for the yawed section becomes

$$c_{dp_y} = \frac{D_{p_y}}{\frac{1}{2}\rho_\infty V_\infty^2 S} = c_{dp_{(\Lambda=0)}} \cos^3\Lambda. \tag{20}$$

As noted previously (see Fig. 11), the pressure drag dominates in reverse flow (97% of the total drag at $\alpha = 172°$, $M = 0.6$ and $\Lambda = 0°$). It can reasonably be assumed that $c_{dp} \simeq c_d$ and $c_{dp_{(\Lambda=0)}} \simeq c_{d_{2D}}$, so that the yawed pressure drag coefficient can be written as

$$c_{d_y} = c_{d_{2D}} \cos^3\Lambda. \tag{21}$$

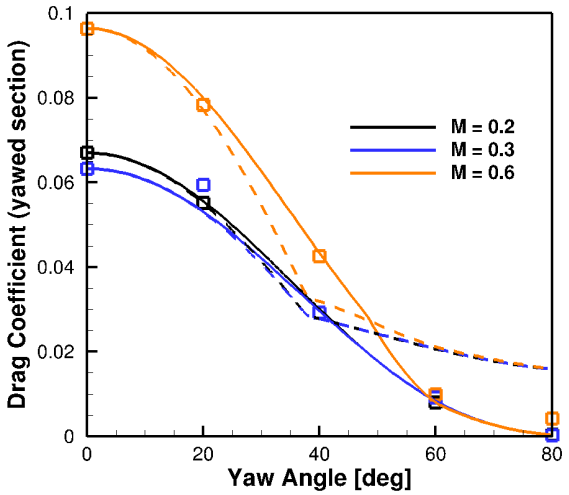

Fig. 13: Correlation of the drag coefficient of an infinite NACA0012 wing in reverse flow ($\alpha = 172°$) predicted using the crossflow model with (solid line) and without (dash lines) pressure drag correction, and CFD data (symbols).

The drag coefficients predicted by the crossflow model (Eq. (12)) and pressure correction (Eq. (21)) are correlated with the numerical experiments in Fig. 13. In reverse flow ($|\alpha| > 90°$), the angle of attack correction for the crossflow model becomes

$$\alpha_y = \left[\left(|\alpha| - 180°\right)\cos^2\Lambda + 180°\right] \text{sign}(\alpha) \tag{22}$$

for the lift and pitching moment coefficient and

$$\alpha_y = \left[\left(|\alpha| - 180°\right)\cos\Lambda + 180°\right] \text{sign}(\alpha) \tag{23}$$

for the drag coefficient [36]. The pressure drag correction provides very good results, consistently within 10% of the CFD data. However, the correction predicts zero drag when $\Lambda = 90°$, because the skin friction has been neglected in Eq. (21). The crossflow model fails significantly at high yaw angles, overpredicting the drag coefficient by 100% at $\Lambda = 80°$. The explanation for this error is simple. As the yaw angle increases, the effective angle of attack α_y converges to $180°$. The drag coefficient at $\alpha = 180°$ is significantly higher than the drag coefficient at $0°$ due to the boundary layer separation at the trailing edge (see Fig. 12). However, the drag coefficients at $180°$ and $0°$ should theoretically be equivalent when $\Lambda = 90°$. This is an inconsistency of the crossflow model that results in the large discrepancies observed in Fig. 13.

5.5 Impact on Rotor Aerodynamics

The impact of the new corrections for the crossflow model on the rotor performance was investigated using the H-34 test data [37]. The NACA0012 untapered, untwisted rotor was modeled using Dymore, a finite element based multibody dynamics code [38]. The present analysis established the impact of the C-81

table discrepancies on a rotor blade during forward flight. This study was conducted at an advance ratio $\mu = 0.4$, for which large yaw angles are expected over the disk. The tip Mach number was chosen to be $M_{\text{tip}} = 0.9$. The control positions and shaft angle of attack were obtained from Harris [2], corresponding to the case $C_T/\sigma = 0.077$. The analysis was performed wth an open loop between the C-81 tables and the aeroelastic response to quantify the aerodynamic effects only. The results from the corrected model were compared with the crossflow model described in Eq. (11) and (12). The lift and drag coefficients are weighed by the Mach number squared, as has become a standard approach of comparing these data. The relative percentage errors between the models are shown in Fig. 14. While some regions have large relative errors, the consequences of the error can remain negligible if the dynamic pressure is locally small (e.g., near the blade root).

The results in Fig. 14 indicate that the corrections have a significant impact on both the lift and drag coefficients. It is readily observed that the error between the two models is at a maximum in regions where the Mach number, sweep angle and angle of attack are highest on the aft side of the rotor disk, close to the tip (Fig 14a). In this region, the lift coefficient (non-weighted) varies by 20% and the drag coefficient by 25% between the standard and the corrected crossflow models. The differences are also significant in the reverse flow region, but their impact is significantly damped by the low local dynamic pressure. The results presented in the section are for a single moderate flight condition. As the aircraft weight increases, so should the blade loading and local angles of attack. Higher advance ratios will result in large regions of crossflow, as depicted in Fig. 1. It is therefore expected that the observed failure of the standard crossflow model will become aggravated as future rotorcraft concepts grow larger and faster.

6 CONCLUSION

In the present study, high fidelity computations with a computational fluid dynamics (CFD) solver on an infinite yawed NACA0012 wing for a wide range of Mach numbers, angles of attack and yaw angles were evaluated for low angles of attack (below 8°) for the range of Mach numbers from incompressible to sonic. These numerical experiments were then used to evaluate the performance of a standard crossflow model at high-advance-ratio flight. Primary conclusions include:

1. A radial basis function can be used to interpolate the airfoil tables to much finer resolution so that fast linear polynomial interpolations can be retained in the present comprehensive codes with-

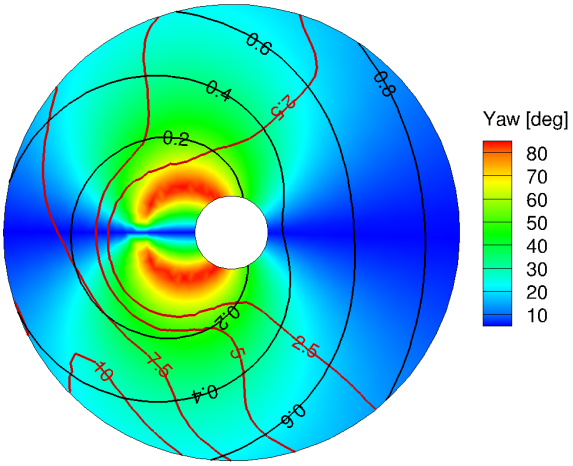

(a) Contours of yaw angle superimposed with lines of Mach number (black) and angle of attack (red). The angles are displayed in degrees.

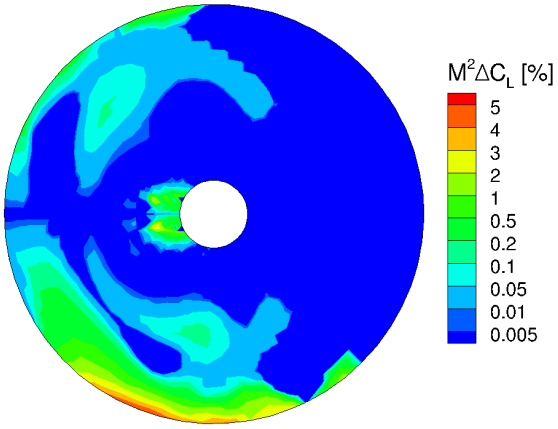

(b) Percent error in lift coefficient

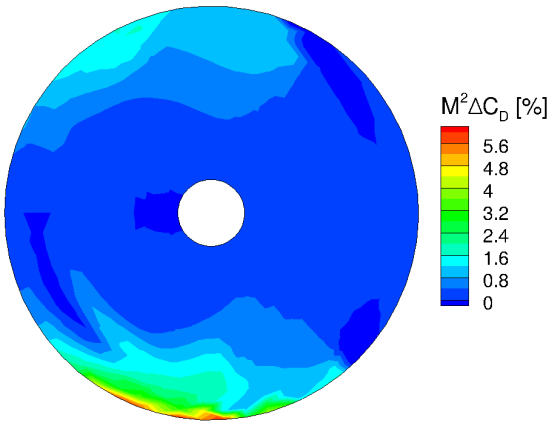

(c) Percent error in drag coefficient

Fig. 14: Relative percentage error between the corrected model and the original crossflow model predictions. The freestream comes from the top and the rotor turns in the counterclockwise direction. Test conditions: $M_{tip} = 0.9$, $\mu = 0.4$, $C_T/\sigma = 0.077$ (H34 rotor)

out the large errors (up to 50%) obtained when significant nonlinear changes are encountered.

2. The independence principle holds for lift coefficient predictions in the linear range of angles of attack for all the Mach numbers and yaw angles investigated in the present study ($M = 0.2 - 0.8$, $\Lambda = 0^\circ - 80^\circ$). However, the crossflow formulation results in significant errors when applied to airfoils in the transonic yawed regime, over predicting the lift coefficient by more than 50%. It is recommended that the model switch from a crossflow to independence principle formulation when transonic flow is encountered. The equation for the critical pressure coefficient or other similar equations can be applied to determine when transonic flow is locally encountered.

3. The assumption that the boundary layer grows in the freestream direction, unaffected by the crossflow was verified with the present numerical experiments. However, it was found that Reynolds number effects due to changes in the reference chord length should be included above $\Lambda \simeq 40^\circ$ in order to obtain accurate predictions. A simple correction $C_{d_y} = C_{d_{2D}} \cos^{1/5} \Lambda$ based on physical arguments is proposed to account for this change.

4. The conclusions obtained for the lift coefficient also apply to the pitching moment coefficient. The independence principle can predict the pitching moment within 10% of the numerical experiments, whereas the crossflow model fails in the transonic regime. This failure is due to the large non-linearities beyond the critical Mach number.

5. For reverse flow at angles of attack with 8° of the relative free stream velocity, independence principle accurately predicts within 10% of the numerical experiments the lift and pitching moment coefficient over the whole range of angles of attack and Mach numbers that were evaluated.

6. The crossflow model fails to accurately predict the drag coefficient in reverse flow, primarily due to the large amount of boundary layer separation. A drag correction, based on physical behavior, was developed to accurately predict the change in pressure drag coefficient with yaw angle: $c_{d_y} = c_{d_{2D}} \cos^3 \Lambda$.

7. Comparison at a moderate advance ratio of 0.4 indicates that errors due to crossflow and reverse flow in both subcritical and transonic Mach regions are significant (up to 25% in lift and drag coefficients). Based on the literature, higher advance ratios of 1.0 – 2.0 will encounter even larger errors if corrections are not applied.

COPYRIGHT STATEMENT

REFERENCES

[1] Carter Jr, J., "High Speed Rotor Aircraft," US Patent 6,435,453, 2002.

[2] Harris, F. D., "Rotor Performance at High Advance Ratio," *NASA CR 215370*, 2008.

[3] Smith, M. J., Koukol, B., Quackenbush, T., and Wachspress, D., "Reverse- and Cross-Flow Aerodynamics for High Advance-Ratio Flight," Proc. of the 35th ERF, 2009.

[4] Purser, P. and Spearman, M., "Wind-Tunnel Tests at Low Speed of Swept and Yawed Wings Having Various Plan Forms," *NACA TN-2445*, 1951.

[5] Harris, F., "Preliminary Study of Radial Flow Effects on Rotor Blades," *Journal of the AHS*, Vol. 11, (3), 1966, pp. 1–21.

[6] St Hilaire, A., Carta, F., Fink, M., and Jepson, W., "Influence of Sweep on the Aerodynamic Loading of an Oscillating NACA 0012 Airfoil," *NASA CR 3092*, 1979.

[7] St Hilaire, A. and Carta, F., "Analysis of Unswept and Swept Wing Chordwise Pressure Data from an Oscillating NACA 0012 Airfoil Experiment," *NASA CR 3567*, 1983.

[8] Lorber, P., Carta, F., and Covino Jr, A., "An Oscillating Three-Dimensional Wing Experiment," *UTRC Report 92-958325-6*, 1992.

[9] McCroskey, W. and Yaggy, P., "Laminar Boundary Layers on Helicopter Rotors in Forward Flight." *AIAA Journal*, Vol. 6, (10), 1968, pp. 1919–1926.

[10] Johnson, W., Yamauchi, G. K., and Watts, M. E., "NASA Heavy Lift Rotorcraft Systems Investigation," *NASA TP 213467*, 2005.

[11] Quakenbush, T. and Wachspress, D., "Measurement and Analysis of High Advance Ratio Rotor Performance," Proc. of the AHS 64th Forum, Montreal, CA, 2008.

[12] Quakenbush, T., Wachspress, D., McKillip, R. M. J., and Sibilia, M. J., "Experimental and Analytical Studies of Lifting Rotor Performance at High Advance Ratios," Proc. of the AHS Aeromechanics Specialists Conference, San Francisco, CA, 2010.

[13] Datta, A., Yeo, H., and Norman, T. R., "Experimental Investigation and Fundamental Understanding of a Slowed UH-60A Rotor at High Advance Ratios," Proc. of the AHS 67th Forum, Virginia Beach, VA, 2011.

[14] Montaudouin, J., Heo, S., Smith, M., and Bauchau, O., "Aerodynamic and Aeroelastic Analysis of Rotors at High Advance Ratio," Proc. of the 36th European Rotorcraft Forum, Paris, France, 2010.

[15] Bowen-Davies, G. and Chopra, I., "Validation of Rotor Performance and Loads at High Advance Ratio," AHS-ASC, San Francisco, CA, 2014.

[16] Quakenbush, T., Wachspress, D., and Smith, M. J., "Next Generation Modeling Technology for High Speed Rotorcraft, SBIR Phase II," Technical report, NASA Ames Research Center, 2011.

[17] McCroskey, W., "A Critical Assessment of Wind Tunnel Results for the NACA 0012 Airfoil," Technical report, NASA TM 100019, 1987.

[18] Jespersen, D., Pulliam, T., and Buning, P., "Recent Enhancements to OVERFLOW," Proc. of the 35th AIAA-ASME (97-0644), Reno, NV, 1997.

[19] Sánchez-Rocha, M. and Menon, S., "The Compressible Hybrid RANS/LES Formulation Using an Additive Operator," *JCP*, Vol. 228, (6), 2009.

[20] Shenoy, R., Holmes, M., Smith, M. J., and Komerath, N. M., "Scaling Evaluations on the Drag of a Hub System," *Journal of the AHS*, Vol. 58, (3), 2013, pp. 1–13.

[21] Lynch, C. E. and Smith, M. J., "Extension and Exploration of a Hybrid Turbulence Model on Unstructured Grids," *AIAA journal*, Vol. 49, (11), 2011, pp. 2585–2591.

[22] Smith, M. J., Liggett, N. D., and Koukol, B. C., "Aerodynamics of Airfoils at High and Reverse Angles of Attack," *Journal of Aircraft*, Vol. 48, (6), 2011, pp. 2012–2023.

[23] Szydlowski, J. and Costes, M., "Simulation of Flow Around a Static and Oscillating in Pitch NACA 0015 Airfoil Using URANS and DES," ASME 2004 Heat Transfer/Fluids Eng. Summer Conf., 2004.

[24] Bousman, W., "Aerodynamic Characteristics of SC1095 and SC1094 R8 Airfoils," Technical Report TP-212265, NASA Ames Research Center, 2003.

[25] Kuchemann, D., *The Aerodynamic Design of Aircraft*, Progress in Aeronautical Sciences, Pergamon Press, New York, NY, 1978.

[26] Jones, R. T., "Effects of Sweepback on Boundary Layer and Separation," *NACA Report 884*, 1947.

[27] Moore, F. K., "Three-Dimensional Boundary Layer Theory," *Advances in Applied Mechanics*, Vol. 4, 1956, pp. 159–228.

[28] Wygnanski, I., Tewes, P., and Taubert, L., "Applying the Boundary-Layer Independence Principle to Turbulent Flows," *Journal of Aircraft*, 2014, pp. 1–8.

[29] Johnson, W., *Helicopter Theory*, Dover Publications, 2012.

[30] Sweet, G. and Jenkins, J., "Results of Wind-Tunnel Measurements on a Helicopter Rotor Operating at Extreme Thrust Coefficients and High-Tip-Speed Ratios," *Journal of the AHS*, Vol. 8, (3), 1963.

[31] Koziel, S. and Leifsson, L., *Surrogate-Based Modeling and Optimization: Applications in Engineering*, Springer Science & Business, 2013.

[32] Smith, M. J., Cesnik, C. E. S., and Hodges, D. H., "Evaluation of Some Data Transfer Algorithms for Noncontiguous Meshes," *Journal of Aerospace Engineering*, Vol. 13, (2), 2000, pp. 52–58.

[33] Gormont, R., "A Mathematical Model of Unsteady Aerodynamics and Radial Flow for Application to Helicopter Rotors," *USAAMRDL TR 72-67*, 1973.

[34] Altman, J. and Hayter, N., "A Comparison of the Turbulent Boundary-layer Growth on an Unswept and a Swept Wing," *NACA TN-2500*, 1951.

[35] Ashkenas, H. and Riddell, F. R., *Investigation of the Turbulent Boundary Layer on a Yawed Flat Plate*, National Advisory Committee for Aeronautics, 1955.

[36] Johnson, W., "A Comprehensive Analytical Model of Rotorcraft Aerodynamics and Dynamics," *NASA TM 81182*, 1980.

[37] McCloud, J., Biggers, J., and Stroub, R., "An Investigation of Full-Scale Helicopter Rotors at High Advance Ratios and Advancing Tip Mach Numbers," *NASA TN D-4632 (605)*, 1968.

[38] Bauchau, O. A., "DYMORE Users Manual," *Georgia Inst. of Technology, Atlanta*, 2007.